

## **$^{119}\text{Sn}$ electric field gradients in model clusters of chalcogenide glasses**

**Jozef Bicerano\***

Energy Conversion Devices, Inc, 1675 West Maple Road, Troy, MI 48084, USA

(Received September 17/Accepted December 18, 1986)

Calculations of  $^{119}\text{Sn}$  electric field gradients (EFG) have been performed using the Extended Hückel approximation on characteristic molecular clusters simulating possible types of sites in chalcogenide glasses. The motivation for these calculations derives from theoretical concepts on varying near neighbor relationships in these types of glasses, and from recent  $^{119}\text{Sn}$  Mössbauer experiments on Sn-doped  $\text{Ge}_x(\text{Se or S})_{1-x}$  bulk glasses which reveal three types (*A*, *B* and *C*) of chemically inequivalent sites, with distinct values and composition dependences for their isomer shifts and quadrupole splittings. The model clusters chosen for the calculations were the ethane-like  $(\text{Ge}_2\text{Se}_3)_n$  quasi-one-dimensional chains of varying lengths which have been proposed as possible sources of the *B* site. In addition, calculations were also carried out on several additional types of clusters, in order to help in interpreting the results for the chains. We find that the magnitude of the quadrupole splitting in isolated linear ethane-like chains is very small, and almost independent of the particular site along the chain at which Sn replaces Ge. It therefore seems unlikely that such isolated linear clusters would be the source of the *B* sites. These sites are more likely to be related to distortions of the ethane-like clusters into non-linear configurations, as well as interactions with neighboring clusters, as forced by the constraints of the packing in the structure of the glass.

**Key words:**  $^{119}\text{Sn}$  — Electric field gradient — Model — Calculation — Mössbauer — Extended Hückel — Packing — Structure — Chalcogenide glasses — Quadrupole splittings

\* *Current address:* Dow Chemical Company, Central Research, Materials Science and Engineered Products Laboratory, 1702 Building, Midland, MI 48674, USA

## 1. Introduction

Interest in chalcogenide glasses was first stimulated nearly two decades ago by the discovery of reversible electronic switching phenomena [1] in many of these glasses. This discovery was followed by the discussion of theoretical concepts on varying near neighbor relationships in these glasses [2]. Recently, the technique of Ag photodoping [3] in these glasses has rapidly emerged because of the high sensitivity and submicron resolution displayed by such materials as photoresists. A basic understanding of these phenomena requires that the microscopic structure of these glasses be firmly established. This problem has been addressed by a variety of techniques such as diffraction methods, vibrational spectroscopy, nuclear quadrupole resonance, and nuclear magnetic resonance, over the years; however, it is only recently that new insight into the morphological structure of these materials has become available by using Mössbauer spectroscopy [4]. These results have extended in a significant manner the structural information on glasses deduced by Raman spectroscopy. In particular, experiments have shown [5] that some of the best glass formers such as  $\text{GeSe}_2$  and  $\text{GeS}_2$  owe their unique glass forming tendency in part to some degree of molecular phase separation into large clusters. These clusters, which are originally present in liquid melts, are believed to be frozen in upon supercooling to form the bulk glasses.

The  $\text{Ge}_x(\text{Se or S})_{1-x}$  binary alloy network glasses are examples of systems exhibiting molecular clustering, with evidence of broken chemical order at stoichiometric compositions ( $x = 1/3$  and  $2/5$ ). This is shown in Fig. 1, which displays the site intensity ratios ( $I_n/I$ ) of the three chemically inequivalent sites (*A*, *B* and *C*) seen using  $^{119}\text{Sn}$  Mössbauer spectroscopy. Based on these  $I_n(x)/I(x)$  systematics, the sites have been ascribed to the presence of Sn replacing Ge in specific molecular clusters. These are layered-like  $\text{Ge}(\text{Se or S})_2$  clusters (type *A* sites), ethane-like  $\text{Ge}_2(\text{Se or S})_3$  chains (type *B* sites), and distorted rocksalt-like  $\text{Ge}(\text{Se or S})$  layered structures (type *C* sites).

A particularly illuminating feature of these Mössbauer experiments is the smooth  $x$ -variation of the nuclear hyperfine parameters (isomer shifts  $\delta$  and quadrupole splittings  $\Delta$ ) of *B* and *C* sites, as depicted in Fig. 2 for  $\text{Ge}_x\text{Se}_{1-x}$  and Fig. 3 for  $\text{Ge}_x\text{S}_{1-x}$ . These results provide general evidence of a glass-composition-induced structural relaxation of the specific clusters. For example, it is well known from macroscopic measurements such as molar volumes that these networks, in general, become more compact (i.e. increase in density) as  $x > 1/3$ .

The aim of this paper is to present a theoretical analysis of the  $x$ -dependence of  $\Delta$  and investigate the underlying molecular structural consequences. The quadrupole splitting  $\Delta$  is related to the EFG tensor through the following usual relation (see Eqs. (1)–(10) and the related discussion in Sect. 2 for more details):

$$\Delta = eQV_{zz}(1 + \eta^2/3)^{1/2}/2.$$

Our approach here is to calculate the EFG tensor in model molecular clusters simulating the *B* clusters of these glasses, using the Extended Hückel approximation. We find that the magnitude of  $\Delta$  in isolated linear ethane-like chains is very

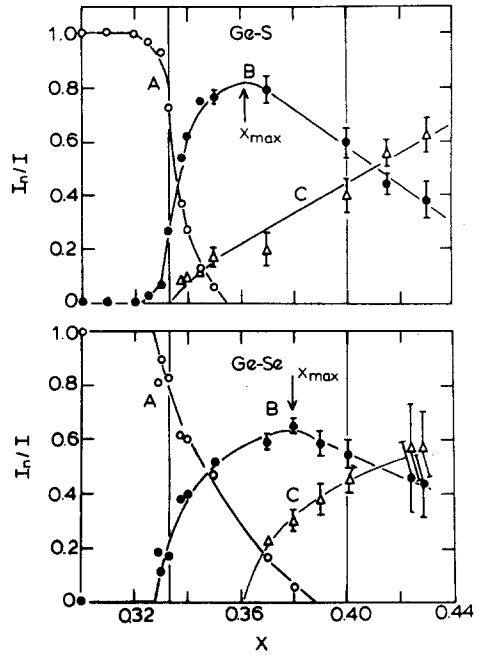


**Fig. 1.** Mössbauer site intensities ( $I_n/I$ ,  $n = A, B$  and  $C$ ) in  $(\text{Ge}_{0.99}\text{Sn}_{0.01})_x\text{X}_{1-x}$  melt-quenched glasses for  $X = \text{S}$  (top figure) and  $X = \text{Se}$  (bottom figure) [5b]

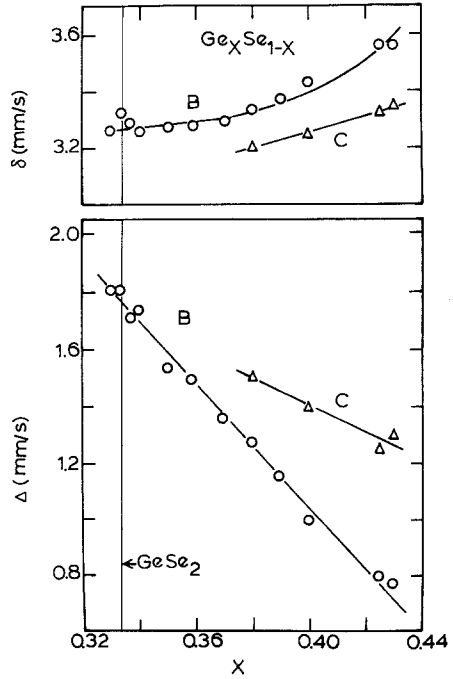


**Fig. 2.**  $^{119}\text{Sn}$  isomer shifts ( $\delta$ ) and quadrupole splittings ( $\Delta$ ) of the  $B$  and  $C$  sites in  $(\text{Ge}_{0.99}\text{Sn}_{0.01})_x\text{Se}_{1-x}$  melt-quenched glasses [5c]

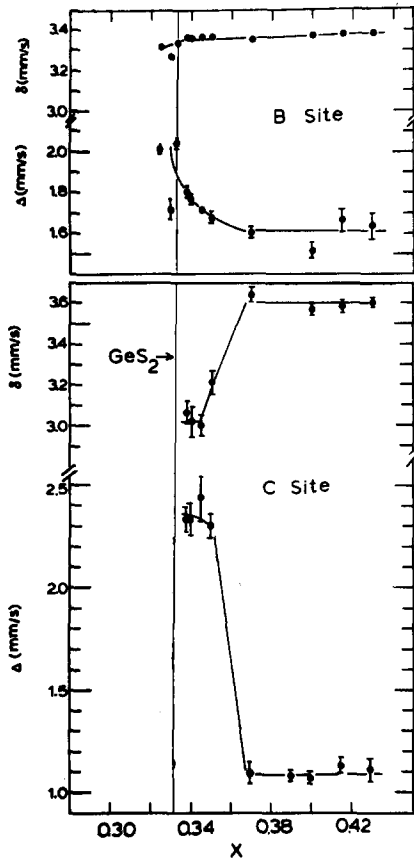


Fig. 3.  $^{119}\text{Sn}$  isomer shifts ( $\delta$ ) and quadrupole splittings ( $\Delta$ ) of the *B* and *C* sites in  $(\text{Ge}_{0.99}\text{Sn}_{0.01})_x\text{S}_{1-x}$  melt-quenched glasses [5b]

small, and almost independent of the particular site along the chain at which Sn replaces Ge. Such isolated linear clusters cannot, therefore, be the source of the *B* sites. These sites are more likely to be related to distortions of the ethane-like clusters into non-linear configurations, as well as interactions with close-by neighboring clusters, as forced by the constraints of the packing in the structure of the glass.

The theoretical procedures used and the results obtained are outlined in Sect. 2. The results of the theoretical calculations and of related experiments are discussed in Sect. 3.

## 2. Theoretical procedures and results

### 2.1. The model clusters

2.1.1. Ethane-like  $\text{Ge}_2\text{Se}_3$  chains. The first type of model cluster considered was linear ethane-like  $\text{Ge}_2\text{Se}_3$  quasi-one-dimensional chains of different lengths, as

shown schematically in Fig. 4. In the shorter chains ( $\text{Ge}_6\text{Se}_9\text{H}_2$ ), the third Ge was replaced by an Sn. In the longer chains ( $\text{Ge}_{14}\text{Se}_{21}\text{H}_2$ ), the effect of substituting Sn for Ge in the second through seventh Ge sites respectively, was examined, to learn about the position and composition dependence of  $V_{zz}$  and  $\Delta$ . The two hydrogen atoms were used to tie up the “dangling bonds” on the two terminal Ge atoms as unobtrusively as possible, in order to get the proper electron configuration for the clusters. These clusters have the advantages of having the proper backbone stoichiometry of  $(\text{Ge}_2\text{Se}_3)_n$ , and of needing the fewest possible number of dangling bond terminators (only two). They are therefore better models of the  $(\text{Ge}_2\text{Se}_3)_n$  chains than clusters terminated by  $\text{GeH}_3$  groups or by Se-H bonds. In any case, preliminary calculations showed that the results are quite similar when these alternative chain terminations are used.

The bond lengths were generally taken to be equal to the sum of the covalent radii [6] of the atoms involved, thus giving  $r(\text{Ge-Sn}) = 2.63 \text{ \AA}$ ,  $r(\text{Ge-Ge}) = 2.44 \text{ \AA}$ ,  $r(\text{Ge-Se}) = 2.38 \text{ \AA}$ , and  $r(\text{Sn-Ge}) = 2.57 \text{ \AA}$ . In the triple bridges of Se atoms, each Se was kept at  $3.8 \text{ \AA}$  from the other two. Since the Van der Waals radius [6] of Se is  $2.0 \text{ \AA}$ , this Se-Se distance, which is very close to twice the Van der Waals radius of Se ( $4.0 \text{ \AA}$ ), ensures that the Se atoms will not interact strongly with one another, but mainly through weak Van der Waals interactions, while the angles around the Ge or Sn atom will not be distorted too much from the tetrahedral angle.

The only exceptions to taking bond lengths equal to the values quote in the previous paragraph, were made for the Ge-Se bonds occurring between triply bridged Ge and Sn, or Ge and Ge atoms. In these cases, the Ge location was chosen by taking the arithmetic mean of two extreme cases:

- (i) When  $r(\text{Ge-Se}) = 2.38 \text{ \AA}$ ;
- (ii) When Ge is exactly as distorted as Sn, i.e. at an Se-Ge-Se angle of  $95.34^\circ$  and Ge-Se distance of  $2.57 \text{ \AA}$ . The locations thus obtained for Ge had Se-Ge-Se angles of  $100.68^\circ$ ,  $r(\text{Ge-Se}) = 2.4681 \text{ \AA}$ , and  $r(\text{Sn-Ge}) = 2.469 \text{ \AA}$  if the other end of the triple bridge contained an Sn atom, or  $r(\text{Ge-Ge}) = 2.261 \text{ \AA}$  if the other end contained another Ge.

Although it may, at first sight, seem that this type of cluster allows the Group IV atoms, which are not directly bonded, but only linked through three Se bridges, to come too close to one another, this is not the case. For example, in the  $\text{SnGe}_3\text{Se}_9\text{H}_2$  cluster, the Sn atom at position 3 and the Ge atom at position 4 are at a distance of  $2.469 \text{ \AA}$  from one another. This is smaller than  $2.63 \text{ \AA}$ , which is

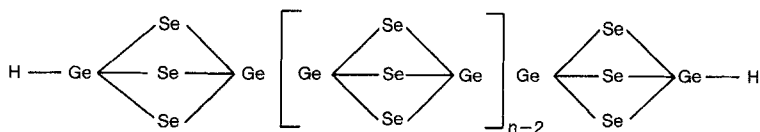


**Fig. 4.** A schematic illustration of the ethane-like  $\text{H}(\text{GeSe}_3\text{Ge})_n\text{H}$  quasi-one-dimensional clusters. Different values of  $n$  give different lengths for the chains. For example,  $\text{Ge}_6\text{Se}_9\text{H}_2$  is obtained for  $n = 3$ , and  $\text{Ge}_{14}\text{Se}_{21}\text{H}_2$  is obtained for  $n = 7$

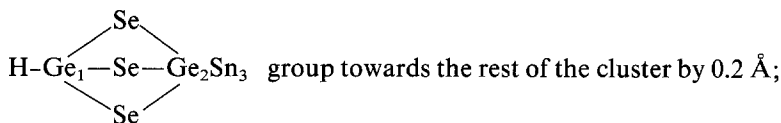
the sum of the covalent radii of Sn and Ge. The solution to this apparent paradox is that  $^{119}\text{Sn}$  Mössbauer isomer shifts for the "B" site [3], which is being conjectured to be related to these ethane-like clusters, indicate that Sn is nominally  $\text{Sn}^{2+}$ , which has a radius [7] of 0.93 Å, and Ge is close to being nominally  $\text{Ge}^{2+}$ , which has a radius [7] of 0.73 Å. The sum of these ionic radii (1.66 Å) is quite compatible with the Sn and the Ge atoms being at 2.469 Å from one another, but not bonded to each other. The same type of argument also holds for non-bonded Ge-Ge pairs at a distance of 2.261 Å, connected only by three Se bridges, since two times the radius of  $\text{Ge}^{2+}$  is equal to 1.46 Å.

The neighboring  $\text{Se}_3$  groups can either be mutually staggered or eclipsed, as in an ethane molecule. The staggered conformation in ethane is more stable by 2.875 kcal/mole [8]. It is difficult to reliably determine such small energy differences by Extended Hückel calculations. Calculations on both conformations of  $\text{SnGe}_5\text{Se}_9\text{H}_2$  gave very similar  $\Delta$  values, and the calculations on all the other clusters were carried out with mutually staggered  $\text{Se}_3$  groups.

The bond distance between the terminal Ge and H atoms was chosen to be the same as the Ge-H bond distance in the chlorogermane ( $\text{GeH}_3\text{Cl}$ ) molecule [9], namely,  $r(\text{Ge-H}) = 1.52$  Å.

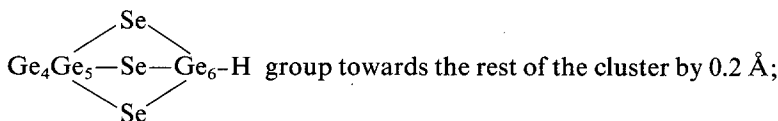
The effect of several small atomic displacements along the axis of threefold rotational symmetry on  $\Delta$  was also examined for the  $\text{SnGe}_5\text{Se}_9\text{H}_2$  cluster:

(i) Move the



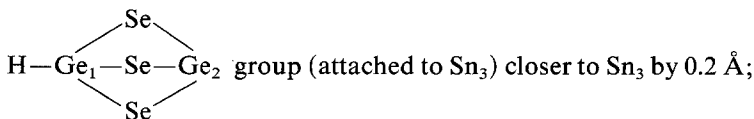
(ii) Move it away by 0.2 Å

(iii) Move the



(iv) Move it away by 0.2 Å;

(v) Move only the



(vi) Move it further by 0.2 Å.

Finally, for intermediate-length  $\text{SnGe}_7\text{Se}_{15}$  clusters, a set of calculations was carried out in which the dangling bonds were tied up, not by terminal H atoms, but by reducing the pyramidal angles at the ends and bringing the terminal Se

atoms to within the Se–Se distance observe in crystalline Se (2.321 Å) from each other. All the other bond lengths and angles were kept as above. This not only ties up the dangling bonds, but overcompensates for them by making the terminal Se atoms formally trivalent. If this type of mechanism were to tie up the dangling bonds, the three formal bonds around the terminal Se atoms would probably each be slightly weaker (and longer) than a regular full single bond. These clusters do not give the correct electron configuration, and will not be considered any further.

2.1.2. Ethane-like  $\text{Sn}_2\text{S}_3$  chains. Calculations were also carried out on a staggered linear ethane-like  $\text{Sn}_{14}\text{S}_{21}\text{H}_2$  cluster representative of possible ethane-like clusters in  $\text{Sn}_x\text{S}_{1-x}$  bulk glasses, in order to determine if any significant changes would occur in the Mössbauer parameters as compared to the  $\text{Ge}_x\text{Se}_{1-x}$  glasses, due to the much larger size difference between Sn and S.

The bond lengths of the bonds in the backbone were taken to be equal to the sum of the covalent radii [6] of the atoms involved, thus giving  $r(\text{Sn}-\text{Sn}) = 2.80$  Å and  $r(\text{Sn}-\text{S}) = 2.45$  Å. The Sn–H bond distance was assumed to be 1.783 Å, as in Subsection 2.1.4. for the small molecules. In the triple bridges of S atoms, each S was kept at 3.5 Å from the other two, i.e. very close to twice the Van der Waals radius [6] of S ( $2 \times 1.85$  Å = 3.7 Å).

2.1.3. Clusters simulating hexagonal  $\text{SnS}_2$ . Next, clusters simulating the hexagonal  $\text{SnS}_2$  structure were examined. In this material, which has a simple  $\text{CdI}_2$  or brucite-type structure [10], layers of distorted  $\text{SnS}_6$  octahedra are the principal structural units. In these distorted octahedra, although all the Sn–S distances are equal, the S–S distances are not. The layers are held together by weaker Van der Waals forces.

Three model clusters were considered:

- (i)  $\text{SnS}_6^{8-}$ , i.e. a central Sn atom surrounded by its six S neighbors, with the overall ionic charge of  $-8$  being used to compensate for the fact that the cluster does not have the correct stoichiometry ( $\text{SnS}_2$ ), and to enable the proper electron configuration to be obtained, by filling all the low-lying molecular orbitals which would be filled if there were a sufficient number of Sn atoms;
- (ii)  $\text{Sn}_7\text{S}_{24}^{20-}$ , i.e. the central Sn atom surrounded by its six nearest Sn neighbors at a distance of 3.638 Å on the same layer, each of the seven Sn atoms being surrounded by its distorted octahedron of six S neighbors, and an overall stoichiometry-compensating ionic charge of  $-20$ ;
- (iii)  $\text{Sn}_{19}\text{S}_{54}^{32-}$ , i.e. the six nearest Sn neighbors also surrounded by their own full set of Sn neighbors on the same layer, each of the 19 Sn atoms being surrounded by its distorted octahedron of six S neighbors, and an overall stoichiometry-compensating ionic charge of  $-32$ . (See Fig. 5 for the Sn arrangement in these clusters, where the Mössbauer isotope was always assumed to be the central Sn atom.)

It is worth noting that according to our preliminary calculations, the large negative charges assumed on these clusters in order to correct their non-stoichiometric

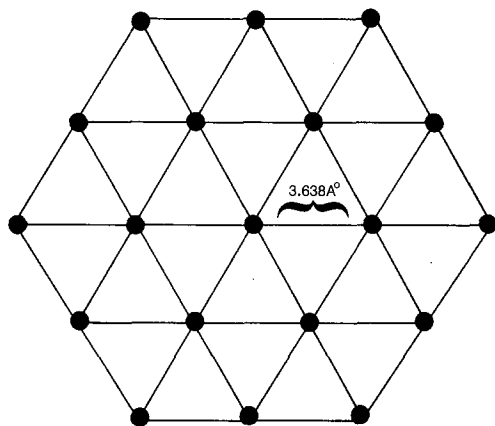


**Fig. 5.** The arrangement of Sn atoms in the clusters representing the hexagonal  $\text{SnS}_2$  structure. Only the central Sn is included in the  $\text{SnS}_6^{8-}$  cluster. Its six Sn-type neighbors are also included in  $\text{Sn}_7\text{S}_{24}^{20-}$ .  $\text{Sn}_{19}\text{S}_{54}^{32-}$ , in turn, also includes all their Sn-type neighbors, namely, the twelve atoms on the perimeter of the outer hexagon. Each Sn is fully surrounded by its distorted coordination octahedron of six S atoms

characters and to get the correct electron configurations, actually make a relatively small difference in the electronic environments in the immediate vicinity of the Sn atoms, and therefore on their Mössbauer parameters. This is because the extra electrons primarily go into the S lone pair orbitals at the top of the valence band, giving the S atoms their proper overall negative Mulliken charges. The Mulliken orbital populations of the Sn atoms change very little. In addition, since *all* of the S atoms become more negative, there is no significant preferential creation of an additional electric field gradient in any specific direction.

2.1.4. Small molecules. Finally, the following calculations were carried out on small molecules, to gain further understanding into the effects of substitution or geometrical distortion:

- (i)  $\text{SnH}_4$  and  $\text{SnF}_4$  with several bond length or bond angle distortions;
- (ii)  $\text{SnH}_3$ ,  $\text{SnH}_2$ ,  $\text{SnF}_3$ , and  $\text{SnF}_2$ ;
- (iii)  $\text{SnH}_3\text{F}$ ,  $\text{SnH}_2\text{F}_2$ , and  $\text{SnHF}_3$ ; and
- (iv)  $\text{Sn}(\text{SiH}_3)_3$ ,  $\text{SnH}(\text{SiH}_3)_3$ , and  $\text{SnF}(\text{SiH}_3)_3$ .

In these calculations, the following bond distances were assumed before any distortions were applied:

- (i)  $r(\text{Sn-H}) = 1.783 \text{ \AA}$  in  $\text{SnH}_4$ ,  $\text{SnH}_3\text{F}$ ,  $\text{SnH}_2\text{F}_2$ ,  $\text{SnHF}_3$ , and  $\text{SnH}(\text{SiH}_3)_3$ ;
- (ii)  $r(\text{Sn-H}) = 1.8045 \text{ \AA}$  in  $\text{SnH}_3$  and  $1.826 \text{ \AA}$  in  $\text{SnH}_2$ ;
- (iii)  $r(\text{Sn-F}) = 1.874 \text{ \AA}$  in  $\text{SnF}_4$ ,  $\text{SnH}_3\text{F}$ ,  $\text{SnH}_2\text{F}_2$ ,  $\text{SnHF}_3$ , and  $\text{SnF}(\text{SiH}_3)_3$ ;
- (iv)  $r(\text{Sn-F}) = 1.892 \text{ \AA}$  in  $\text{SnF}_3$  and  $1.910 \text{ \AA}$  in  $\text{SnF}_2$ , where the Sn-F distance in  $\text{SnF}_2$  is the experimental value [11].
- (v)  $r(\text{Sn-Si}) = 2.5168 \text{ \AA}$  and  $r(\text{Si-H}) = 1.48 \text{ \AA}$  in  $\text{Sn}(\text{SiH}_3)_3$ ,  $\text{SnH}(\text{SiH}_3)_3$ , and  $\text{SnF}(\text{SiH}_3)_3$ . The  $r(\text{Si-H})$  distance used is the same as the experimental value in silane ( $\text{SiH}_4$ ) [9].

Judiciously chosen values were used for those bond lengths for which experimental values were not available. Tetrahedral bond angles were used for all fourfold-coordinated Sn and Si atoms, as well as for the Sn atom in  $\text{Sn}(\text{SiH}_3)_3$ .



The geometries of  $\text{SnH}_3$  and  $\text{SnF}_3$  are expected to be pyramidal, with a pyramidal angle very close to that of a perfect tetrahedron ( $180^\circ - 109.471^\circ = 70.529^\circ$ ). The pyramidal angles of  $\text{SnH}_3$  and  $\text{SnF}_3$  were assumed to be  $71^\circ$ , in analogy with the experimental value [12] for  $\text{SiF}_3$ . The bond angles of  $\text{SnH}_2$  and  $\text{SnF}_2$  were taken to be  $94^\circ$ , which is the experimental value [11] for  $\text{SnF}_2$ .

The following distortions were applied to  $\text{SnH}_4$  and  $\text{SnF}_4$ :

- (i) Decrease or increase one bond distance by  $0.1 \text{ \AA}$ ;
- (ii) Keep the bond distances equal, but reduce the symmetry to  $C_{3v}$  by distorting the bond angles in the lower  $\text{SnH}_3$  and  $\text{SnF}_3$  portions to  $105.593^\circ$  or  $113.349^\circ$ .

## 2.2. The quantum mechanical calculations

The quantum mechanical calculations were all carried out, using the FORTICON8 software package [13], implementing the Extended Hückel method [14], on an IBM 3033U computer.

The orbital exponents and Coulomb integrals used are listed in Table 1. The parameters for Ge, Sn, S, and Se were taken from the non-relativistic parameterization [15] of Desclaux' atomic Dirac-Fock calculations [16]. The default values given by the FORTICON8 program [13] were used for H, F, and Si. Trial calculations with alternative parameterizations showed that the calculated quadrupole splittings were quite insensitive to the choice made between reasonable parameterizations.

For the  $\text{SnGe}_5\text{Se}_9\text{H}_2$  cluster, the effect of the closed shell of  $4d$  orbitals on Sn and  $3d$  orbitals on Ge was examined by carrying our calculations with and without these orbitals, and their effect was found to be negligibly small, with  $|\Delta|$  differing only by 0.027 between the two calculations. Since the computations took a relatively small amount of computer time, the  $d$  orbitals were retained in all of the remaining calculations on the linear ethane-like clusters, as well as being used in the  $\text{Sn}(\text{SiH}_3)_3$ ,  $\text{SnH}(\text{SiH}_3)_3$  and  $\text{SnF}(\text{SiH}_3)_3$  clusters.

**Table 1.** Orbital exponents and coulomb integrals<sup>a</sup>

Atom	<i>s</i> orbitals			<i>p</i> orbitals			<i>d</i> orbitals		
	<i>n</i>	exp	coul	<i>n</i>	exp	coul	<i>n</i>	exp	coul
Si	3	1.383	-17.3	3	1.383	-9.2	3	1.383	-6.0
Ge	4	2.024	-15.16	4	1.550	-7.329	3	4.853	-44.64
Sn	5	2.129	-13.04	5	1.674	-6.764	4	4.166	-37.38
S	3	2.035	-24.02	3	1.691	-11.6	—	—	—
Se	4	2.409	-22.86	4	1.949	-10.68	—	—	—
F	2	2.425	-40.0	2	2.425	-18.1	—	—	—
H	1	1.3	-13.606	—	—	—	—	—	—

<sup>a</sup> *n* denotes the principal quantum number, exp the orbital exponent, and coul the coulomb integral

### 2.3. The calculation of quadrupole splittings

In general, the calculation of the quadrupole splitting ( $\Delta$ ) [17, 18] requires the evaluation of the elements of the electric field graient (EFG) tensor, and the diagonalization of this tensor. These elements are given as sums of nuclear and electronic contributions:

$$V_{ij} = V_{ij}^{\text{nuc}} + V_{ij}^{\text{el}}, \quad \text{where } i, j = [x, y, z] \quad (1)$$

$$V_{ij}^{\text{nuc}} = \sum_A Z_A (3R_{Ai}R_{Aj} - \delta_{ij}R_A^2) / R_A^5 \quad (2)$$

$$V_{ij}^{\text{el}} = -\langle \Psi | \sum_k (3r_{ki}r_{kj} - \delta_{ij}r_k^2) / r_k^5 | \Psi \rangle. \quad (3)$$

In these equations,  $Z_A$  denotes the nuclear charge of atom A,  $R_A$  denotes its distance from the Mössbauer-active nucleus with respect to which all coordinates  $R_A$  and  $r_k$  are being measured, and  $\Psi$  is the electronic wave function for the cluster. In our calculations, several simplifications can be made:

(i) The EFG tensor at the Mössbauer isotope is already diagonal for all of our clusters, since the off-diagonal elements vanish by symmetry.

(ii) The electronic contributions can be replaced by the “internal” contributions  $V_{ii}^{\text{int}}$  due to the asymmetry of the electron distribution around the Mössbauer isotope itself. These will normally be the major contributions. They can be calculated in terms of the orbital populations  $e(x)$ ,  $e(y)$ ,  $e(z)$ ,  $e(xy)$ , etc., at the Mössbauer isotope, as obtained for the  $p_x$ ,  $p_y$ ,  $p_z$ ,  $d_{xy}$ , etc., orbitals, by a Mulliken population analysis [17].

(iii) Since the other atoms are relatively far away,  $V_{ii}^{\text{nuc}}$  can be replaced by  $V_{ii}^{\text{ext}}$ , the “external” component, which differs from  $V_{ii}^{\text{nuc}}$  because the nuclear charge  $Z_A$  has been replaced by the net Mulliken atomic charge  $q_A$ . In other words, the asymmetry of the charge distribution in the remainder of the lattice is treated by a point charge model, with net Mulliken atomic charges as the point charges located at the nuclear positions. This can be viewed as a generalization of the ion-lattice separation often used for ionic complexes, where the contributions to the EFG are partitioned into contributions from the valence electrons of the atom and from surrounding ions. Similar considerations have been previously applied to the calculation of  $^{125}\text{Te}$  quadrupole interactions for Te atoms and chains present, as substitutional impurities in selenium chains and in selenium and sulfur rings, using the Extended Hückel method [18].

(iv) Since the EFG tensor is a traceless tensor,  $V_{xx} + V_{yy} + V_{zz} = 0$ , so that there are really only two independent parameters needed to specify this tensor completely. These can be chosen as the largest component  $V_{zz}$  and an asymmetry parameter  $\eta$  is defined as:

$$\eta = |(V_{xx} - V_{yy}) / V_{zz}|. \quad (4)$$

The relevant equations then become:

$$V_{zz}^{\text{int}} = \frac{2}{5} \langle r_{5p}^{-3} \rangle [-2e(z) + e(x) + e(y)] \\ + \frac{2}{7} \langle r_{4d}^{-3} \rangle [2e(x^2 - y^2) - 2e(z^2) + 2e(xy) - e(xz) - e(yz)] \quad (5)$$

$$(V_{xx}^{\text{int}} - V_{yy}^{\text{int}}) = \frac{6}{5} \langle r_{5p}^{-3} \rangle [-e(x) + e(y)] - \frac{6}{7} \langle r_{4d}^{-3} \rangle [e(xz) - e(yz)] \quad (6)$$

and

$$V_{ii}^{\text{ext}} = \sum_A q_A (3R_{Ai}^2 - R_A^2) / R_A^5 \quad (7)$$

Here,  $\langle r_{5p}^{-3} \rangle$  and  $\langle r_{4d}^{-3} \rangle$  are the expectation values of  $1/r^3$  for the  $5p$  and  $4d$  orbitals of Sn. (In calculations where the  $d$  orbitals are not included, the terms referring to them in equations (5) and (6) are omitted.) For the total field, we get:

$$V_{zz} = (1 - R) V_{zz}^{\text{int}} + (1 - \gamma_\infty) V_{zz}^{\text{ext}} \quad (8)$$

$$(V_{xx} - V_{yy}) = (1 - R)(V_{xx}^{\text{int}} - V_{yy}^{\text{int}}) + (1 - \gamma_\infty)(V_{xx}^{\text{ext}} - V_{yy}^{\text{ext}}), \quad (9)$$

where the Sternheimer factors  $R$  and  $\gamma_\infty$  represent the effects of shielding and anti-shielding respectively of the nucleus by the core electrons [17].

For an Sn nucleus, which has a spin of  $1/2$  in its ground state and  $3/2$  in its excited state, the interaction of the  $V_{zz}$  component of the EFG with the nuclear quadrupole moment  $eQ$  produces two energy levels with the following separation ( $\Delta$ ) between them:

$$\Delta = eQV_{zz}(1 + \eta^2/3)^{1/2}/2 \quad (10)$$

By using appropriate conversion factors, this quantity can be converted from energy units to mm/sec.

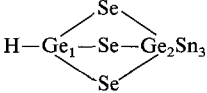
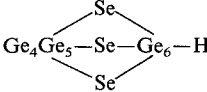
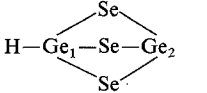
The following values were used for the Sn parameters in our calculations:  $\langle r_{5p}^{-3} \rangle = 78.125 \text{ \AA}^{-3}$ ;  $\langle r_{4d}^{-3} \rangle = 161.574 \text{ \AA}^{-3}$ ;  $R = 0.1$ ;  $\gamma_\infty = -10$ ;  $Q = -0.065$  barns. The values of these parameters were chosen as follows: The EFG for a  $5p_z$  electron [19] in Sn is equal to  $-\frac{4}{5}e\langle r_{5p}^{-3} \rangle = -3.0 \times 10^{16}$  esu. Since  $e = 4.8 \times 10^{-10}$  esu of charge, we get  $\langle r_{5p}^{-3} \rangle = 7.8125 \times 10^{-25} \text{ cm}^{-3} = 78.125 \text{ \AA}^{-3}$ . It has been suggested [20] that  $\langle r_{5p}^{-3} \rangle = 45.5544 \text{ \AA}^{-3}$  and  $\langle r_{4d}^{-3} \rangle = 94.2133 \text{ \AA}^{-3}$ ; however, we have accepted the value  $78.125 \text{ \AA}^{-3}$  for  $\langle r_{5p}^{-3} \rangle$ . Thus, if we scale the  $\langle r_{4d}^{-3} \rangle$  value by  $78.125/45.5544$ , we get  $\langle r_{4d}^{-3} \rangle = 161.574 \text{ \AA}^{-3}$ . The value that we have assumed for  $R(0.1)$  may be slightly underestimated.  $\gamma_\infty$  has been assumed to have the same value as the one estimated [21] for  $\text{Sn}^{4+}$ . Finally, a  $\gamma$ -decay energy of 23.875 keV was used in converting the splittings to units of mm/sec [17].

Table 2 lists the clusters used, their brief descriptions and symmetry point groups, the orbital set used for each calculation, and the values of  $V_{zz}$ ,  $\eta$ ,  $\Delta$ , and  $F = (1 - \gamma_\infty) V_{zz}^{\text{ext}} / (1 - R) V_z^{\text{int}}$ . (This last quantity tells us the relative sign and magnitude of the ‘‘external’’ or lattice terms as compared to the ‘‘internal’’ terms related to distortions of the charge distribution immediately around the M\"ossbauer-active nucleus, after taking the shielding and anti-shielding effects into account.)

### 3. Discussion

The results of our calculations (see Table 2) show that in the ethane-like  $\text{SnGe}_5\text{Se}_9\text{H}_2$ ,  $\text{SnGe}_{13}\text{Se}_{21}\text{H}_2$ , and  $\text{Sn}_{14}\text{S}_{21}\text{H}_2$  clusters, the magnitude of  $\Delta$  is very small, and almost independent of the particular site along the chain at which an Sn atom is located. In fact, starting from the third or fourth site along the longer

Table 2. Clusters and results of calculations

Cluster	Symmetry	Description	$V_{zz}^a$	$\eta^b$	$\Delta^c$	$F^d$
SnGe <sub>5</sub> Se <sub>9</sub> H <sub>2</sub>	$C_{3v}$	Sn replacing Ge <sub>3</sub>	0.289	0.0	-0.035	-1.17
	$C_{3v}$	Eclipsed, Sn replacing Ge <sub>3</sub>	0.281	0.0	-0.034	-1.16
	$C_{3v}$	Sn replacing Ge <sub>3</sub> , no <i>d</i> orbitals	0.059	0.0	-0.007	-1.03
$C_{3v}$		H—Ge <sub>1</sub> —Se—Ge <sub>2</sub> Sn <sub>3</sub>	0.469	0.0	-0.057	-1.22
		group moved closer to Ge <sub>4</sub> by 0.2 Å				
$C_{3v}$		Same group moved away by 0.2 Å	-0.014	0.0	0.002	-0.99
$C_{3v}$		Ge <sub>4</sub> Ge <sub>5</sub> —Se—Ge <sub>6</sub> —H	0.622	0.0	-0.076	-1.36
		group moved closer to Sn <sub>3</sub> by 0.2 Å				
$C_{3v}$		Same group moved away by 0.2 Å	-0.167	0.0	0.021	-0.91
$C_{3v}$		H—Ge <sub>1</sub> —Se—Ge <sub>2</sub>	1.241	0.0	-0.152	-2.21
		group moved closer to Sn <sub>3</sub> by 0.2 Å				
$C_{3v}$		Same group moved away by 0.2 Å	-0.558	0.0	0.068	-0.77
SnGe <sub>13</sub> Se <sub>21</sub> H <sub>2</sub>	$C_{3v}$	Sn replacing Ge <sub>2</sub>	0.434	0.0	-0.053	-1.27
	$C_{3v}$	Sn replacing Ge <sub>3</sub>	0.281	0.0	-0.034	-1.16
	$C_{3v}$	Sn replacing Ge <sub>4</sub> to Ge <sub>7</sub>	0.23	0.0	-0.028	-1.13
Sn <sub>14</sub> S <sub>21</sub> H <sub>2</sub>	$D_{3h}$	Results for Sn <sub>2</sub>	-2.488	0.0	0.305	-0.43
		For Sn <sub>3</sub> to Sn <sub>7</sub>	(-2.695 ± 0.002)	0.0	0.330	-0.40
SnS <sub>6</sub> <sup>8-</sup>	$D_{3d}$	Small SnS <sub>2</sub> -type cluster	-0.042	0.0	0.005	-0.51
Sn <sub>7</sub> S <sub>24</sub> <sup>20-</sup>	$D_{3d}$	Midsized SnS <sub>2</sub> -type cluster	-2.314	0.0	0.283	0.43
Sn <sub>19</sub> S <sub>54</sub> <sup>32-</sup>	$D_{3d}$	Large SnS <sub>2</sub> -type cluster	-2.603	0.0	0.319	0.64
SnH <sub>4</sub>	$T_d$	Tetrahedral H—Sn—H angles (109.471°)	0.0	0.0	0.0	—
	$C_{3v}$	One Sn—H bond shortened by 0.1 Å	-0.568	0.0	0.070	0.20
	$C_{3v}$	One Sn—H bond elongated by 0.1 Å	0.621	0.0	-0.076	0.14
	$C_{3v}$	H—Sn—H angles decreased to 105.593° in lower SnH <sub>3</sub> portion	-0.580	0.0	0.071	0.32
	$C_{3v}$	H—Sn—H angles increased to 113.349° in lower SnH <sub>3</sub> portion	0.638	0.0	-0.078	0.25

Cluster	Symmetry	Description	$V_{zz}^a$	$\eta^b$	$\Delta^c$	$F^d$
SnF <sub>4</sub>	$T_d$	Tetrahedral F-Sn-F angles (109.471°)	0.0	0.0	0.0	—
	$C_{3v}$	One Sn-F bond shortened by 0.1 Å	-0.171	0.0	0.021	-3.44
	$C_{3v}$	One Sn-F bond elongated by 0.1 Å	0.132	0.0	-0.016	-3.13
	$C_{3v}$	F-Sn-F angles decreased to 105.593° in lower SnF <sub>3</sub> portion	-0.282	0.0	0.034	40.80
	$C_{3v}$	F-Sn-F angles increased to 113.349° in lower SnF <sub>3</sub> portion	0.283	0.0	-0.035	16.50
SnH <sub>3</sub>	$C_{3v}$	Pyramidal	9.187	0.0	1.124	-0.09
SnH <sub>2</sub>	$C_{2v}$	Bent (94° bond angle)	-21.284	0.701	2.810	0.02
SnF <sub>3</sub>	$C_{3v}$	Pyramidal	-12.291	0.0	1.504	-0.11
SnF <sub>2</sub>	$C_{2v}$	Bent (94° bond angle)	-14.810	0.184	1.822	0.04
SnH <sub>3</sub> F	$C_{3v}$	Tetrahedral bond angles	6.445	0.0	-0.789	-0.08
SnH <sub>2</sub> F <sub>2</sub>	$C_{2v}$	Tetrahedral bond angles	-6.235	0.939	0.868	-0.08
SnHF <sub>3</sub>	$C_{3v}$	Tetrahedral bond angles	-5.857	0.0	0.717	-0.09
Sn(SiH <sub>3</sub> ) <sub>3</sub>	$C_{3v}$	Tetrahedral bond angles	6.318	0.0	-0.773	-0.004
SnH(SiH <sub>3</sub> ) <sub>3</sub>	$C_{3v}$	Tetrahedral bond angles	5.363	0.0	-0.656	-0.21
SnF(SiH <sub>3</sub> ) <sub>3</sub>	$C_{3v}$	Tetrahedral bond angles	12.408	0.0	-1.518	-0.13

<sup>a</sup> The major component  $V_{zz}$  of the electric field gradient tensor, in units of  $10^{15}$  esu

<sup>b</sup> The asymmetry parameter. Note that this is equal to zero for most of our clusters, because the  $x$  and  $y$  axes are degenerate by symmetry in all the clusters with a threefold symmetry axis, giving  $V_{xx} = V_{yy}$  and therefore  $\eta = 0.0$

<sup>c</sup> Quadrupole splitting, in mm/sec

<sup>d</sup>  $F = (1 - \gamma_{\infty})V_{zz}^{ext}/(1 - R)v_{zz}^{int}$

chains, the results are identical for all “inner” sites for the number of decimal places reported. Furthermore, the results on SnGe<sub>2</sub>Se<sub>2</sub>H<sub>2</sub> also show that the value of  $\Delta$  changes little under considerable (0.2 Å) stretches and compressions of bonds along the threefold axis. This smallness of the values of  $\Delta$  is mostly due to the fact that  $(1 - \gamma_{\infty})V_{zz}^{ext}$  and  $(1 - R)V_{zz}^{int}$  have opposite signs and comparable magnitudes. For example, for the SnGe<sub>13</sub>Se<sub>21</sub>H<sub>2</sub> clusters, the average values of these quantities, in units of  $10^{15}$  esu, are approximately 2.02 and -1.74 respectively, giving values of  $F$  (last column of Table 2) close to unity, and total  $V_{zz}$  values which are almost a full order of magnitude smaller than the separate external and internal components. This is not too surprising since the Sn atom in these clusters has a slightly distorted tetrahedral environment with three neighboring Se atoms and one neighboring Ge atom. The bonding of the Sn and S atoms, which have a much larger size difference as well as a somewhat larger electronegativity difference than Ge and Se, causes more distortion in the vicinity of the Sn atoms in Sn<sub>14</sub>S<sub>21</sub>H<sub>2</sub>, resulting in a smaller value of  $|F|$  and larger (but still quite small) values of  $V_{zz}$  and  $\Delta$ .

The results of the calculations show that the statement made in Sect. 2.1 about

those pairs of Group IV atoms which are linked through three Se bridges not being directly bonded in spite of their very short internuclear distances, is indeed correct. The atomic overlap between such bridge-connected pairs of Ge atoms in  $\text{SnGe}_{13}\text{Se}_{21}\text{H}_2$  is an order of magnitude smaller than the atomic overlap between directly bonded Ge atom pairs with a longer internuclear distance. The atomic overlap between such bridge-connected pairs of Sn atoms in  $\text{Sn}_{14}\text{S}_{21}\text{H}_2$  is a factor of 5 to 6 smaller than the atomic overlap between directly bonded Sn atom pairs.

The results on the clusters simulating hexagonal  $\text{SnS}_2$  and the results on the small molecules, all further help to put the results on the ethane-like clusters into proper perspective. We have mentioned, for example, that  $\text{SnS}_2$  has a simple  $\text{CdI}_2$  or brucite-type structure [10], with layers of distorted  $\text{SnS}_6$  octahedra as the principal structural units. The smallest  $\text{SnS}_2$ -type cluster used ( $\text{SnS}_6^{8-}$ ) represents one of these structural units, and gives a very small value for  $\Delta$ . Addition of more atoms, as done sequentially in the  $\text{Sn}_7\text{S}_{24}^{20-}$  and  $\text{Sn}_{19}\text{S}_{54}^{32-}$  clusters, brings out more strongly the distinctiveness of the  $z$  direction from the  $x$  and  $y$  directions, even though the values of  $\Delta$  are still small since the near neighbor environment of a given Sn atom still consists of the same distorted octahedron of S atoms. The difference in the values of  $\Delta$  for the large and the midsize clusters is much smaller than the difference in the values of  $\Delta$  for the midsize and the small clusters, showing the rapid convergence of  $\Delta$  with increasing cluster size. The values of  $\Delta$  in the two larger  $\text{SnS}_2$ -type clusters are comparable to the values in the ethane-like  $\text{Sn}_{14}\text{S}_{21}\text{H}_2$  cluster.

The calculations on various distorted  $\text{SnH}_4$  and  $\text{SnF}_4$  geometries with  $C_{3v}$  symmetry show that a somewhat distorted tetrahedral configuration gives a small value of  $\Delta$ . The  $\Delta$  value for a given distortion is smaller in  $\text{SnF}_4$  than in  $\text{SnH}_4$  because the bonding in  $\text{SnF}_4$  is extremely ionic, resulting in little Mulliken charge on Sn, and therefore, a very small value of  $(1-R)V_{zz}^{\text{int}}$  relative to  $(1-\gamma_\infty)V_{zz}^{\text{ext}}$ . The  $\Delta$  values for  $\text{SnH}_3$ ,  $\text{SnH}_2$ ,  $\text{SnF}_3$  and  $\text{SnF}_2$ , on the other hand, are quite large, and in fact appreciably larger than the  $|\Delta|$  values in  $\text{SnH}_3\text{F}$ ,  $\text{SnH}_2\text{F}_2$  and  $\text{SnHF}_3$ , which have distorted tetrahedral geometries and two different types of ligands with very different electronegativities attached to Sn. The results for  $\text{SnX}(\text{SiH}_3)_3$  can be understood by considering that the ordering of electronegativities of the atoms is  $\text{F} \gg \text{H} > \text{Sn} > \text{Si}$ ; therefore,  $\Delta$  has a negative sign for  $\text{Sn}(\text{SiH}_3)_3$  while it has a positive sign for  $\text{SnH}_3$ . The sign of  $\Delta$  remains negative for  $\text{X} = \text{H}$  or  $\text{F}$ , but  $|\Delta|$  increases considerably for  $\text{X} = \text{F}$  due to the removal of electrons from the vicinity of Sn by the very electronegative F atom, making the charge distribution around Sn even more asymmetric.

The main reason for carrying out these extra calculations is that the results on such smaller molecules are much easier to interpret, and these results clearly show that our computational approach is capable of detecting significant asymmetries in the electronic environment of an Sn atom and giving appropriately large values and qualitatively correct trends for  $V_{zz}$  and  $\Delta$ . The results presented for the ethane-like chains, therefore strongly suggest that *isolated linear* ethane-like clusters cannot be the source of the *B* sites. On the other hand, explanations given previously for the *B* site in terms of  $\text{Ge}_2\text{Se}_3$ -type chains are also quite

compelling and highly plausible. How can these seemingly conflicting findings be reconciled with one another?

The source of this apparent disagreement most probably lies in the facts that (i) the clusters are certainly not isolated in the solid, but on the contrary, can strongly interact with other structural units; and, (ii) these interactions, plus the constraints of the packing, are likely to cause the ethane-like clusters to fold into nonlinear conformations in the glass. For example, it has been hypothesized [5] that the *B*-type clusters in  $\text{GeSe}_2$  and  $\text{GeS}_2$  glasses have stoichiometries of  $\text{Ge}_{20}\text{Se}_{33}$  and  $\text{Ge}_{16}\text{S}_{27}$  respectively. Let us assume, for the sake of argument, that these clusters are not linear but instead, cyclic, with the dangling bonds being terminated by ring closure, and with the Ge atoms located at the vertices of a regular polygon. Since the internal angle  $\Theta(n)$  of a regular polygon with  $n$  vertices is given by the relation  $\Theta(n) = 180 - 360/n$ , we find that the Ge-Ge-Ge angle would be equal to  $162^\circ$  for  $n = 20$  and  $157.5^\circ$  for  $n = 16$ . (See Ref. [2c] for a discussion of some of the general structural considerations in chalcogenide glasses.)

Such a model could also provide an explanation for the recent observation [5b] (see Fig. 3) that in  $\text{Ge}_x\text{S}_{1-x}$  glasses, even though the value of  $\Delta$  decreases rapidly and almost linearly (actually hyperbolically) with increasing  $x$  for  $0.33 < x < 0.38$ , it converges and remains almost constant for  $0.38 < x < 0.43$ . If  $x$  is small, there will be fewer Ge atoms to form the Ge-rich  $(\text{Ge}_2\text{S}_3)_n$  clusters within the  $\text{GeS}_{1-x}$  glass. Even when they are formed, the  $(\text{Ge}_2\text{S}_3)_n$  clusters will have few atoms, and therefore be small. These small unit clusters will be likely to undergo sizable distortions to fit into their environment. [As a model of this, note that the internal angle,  $\Theta(n)$ , rapidly decreases as  $n$  (the number of vertices) decreases in a regular polygon.] On the other hand, as  $x$  increases, much more Ge atoms will become available to form the Ge-rich  $\text{Ge}_2\text{S}_3$  phase, resulting in larger unit clusters with smaller distortions from linearity, and possibly converging to optimally configured large ethane-like clusters.

Intercluster interactions, as well as models for the distortions from linearity likely to occur in ethane-like clusters, should be examined in future work, in order to shed more light into the nature of the *B* sites and of intrinsically broken chemical order in glassy alloys.

*Acknowledgments.* I would like to thank P. Boolchand for suggesting the problem, for many stimulating discussions, and for providing copies of Figs. 1, 2, and 3. I would also like to thank S. R. Ovshinsky for discussions, support and encouragement throughout this project, J. P. deNeufville for many helpful discussions, and E. M. Norman for typing the manuscript.

## References and notes

1. Ovshinsky SR (1968) *Phys Rev Lett* 21:1450
2. (a) Ovshinsky SR (1981) *J. Phys. Colloq C4*, suppl. au no. 10, 42:1095; (b) (1981) *Rev Roum Phys* 26:893; (c) (1985) In: Adler D, Schwartz BB, Steele MC (eds) *Physical properties of amorphous materials*. Plenum Press, New York, pp 105-155

3. deNeufville JP (1974) In: Stuke J, Brenig W (eds) Proc. 5th International Conference on Amorphous and Liquid Semiconductors. Taylor and Francis, London pp 1351–1360
4. (a) Boolchand P (1985) In: Adler D, Schwartz BB, Steele MC (eds) Physical properties of amorphous materials. Plenum Press, New York, pp 221–260; (b) Boolchand P, Grothaus J, Bresser WJ, Suranyi P (1982) Phys Rev B 25:2975; (c) Bresser WJ, Boolchand P, Suranyi P (1986) Phys Rev Lett 56:2493
5. See: (a) Boolchand P, Grothaus J (1984) In: Chadi JD, Harrison WA (eds) Proceedings of the 17th International Conference on the Physics of Semiconductors. Springer, New York, p 833 for GeSe<sub>2</sub>; (b) Boolchand P, Grothaus J, Tenhover M, Hazle MA, Grasselli RK (1986) Phys Rev B 33:5421 for GeS<sub>2</sub>; (c) Boolchand P et al, to be published
6. Pauling L (1960) The nature of the chemical bond, 3rd edn. Cornell University Press, Ithaca, New York, pp 224–225, gives Ge(1.22 Å), Sn(1.40 Å), Se(1.17 Å) and S(1.04 Å). Slightly different values have also been quoted in the literature. We used 1.41 Å for Sn and 1.16 Å for Se. The Van der Waals radii are listed in p 260
7. Sanderson RT (1967) Inorganic chemistry, Reinhold, New York, p 136
8. Lafferty WJ, Plyler EK (1962) J Chem Phys 37:2688
9. Weast RC, Astle MJ (1979) Handbook of chemistry and physics, 60th edn. CRC Press, p F-218
10. Hazen RM, Finger LW (1978) Am Mineral 63:289
11. Hague RH, Hastie JW, Margrave JL (1973) J Mol Spectrosc 45:420
12. (a) Milligan DE, Jacox ME, Guillory WA (1968) J Chem Phys. 49:5330; (b) Ling-Fai Wang J, Krishnan CN, Margrave JL (1973) J Mol Spectrosc 48:346
13. Howell J, Rossi A, Wallace D, Haraki K, Hoffmann R, QCPE, Program No. 344
14. (a) Hoffmann R, J Chem Phys (1963) 39:1397; (b) Hoffmann R, Lipscomb WN J Chem Phys (1962) 36:2179 and 3479; (1963) J Chem Phys 37: 2872
15. Lohr Jr LL, Pyykkö P (1979) Chem Phys Lett 62:333
16. Desclaux J-P (1973) At Data Nucl Data Tables 12:311
17. Greenwood NN, Gibb TC (1971) Mössbauer spectroscopy. Chapman and Hall, London
18. Coker A, Lee T, Das TP (1976) Phys Rev B 13:55
19. Goldanskí VI, Herber RH (1968) Chemical applications of Mössbauer spectroscopy. New York, Academic Press, pp 321–322
20. Jena P: Theoretical values, private communication
21. Borsa F, Barnes RG (1964) Phys Rev Lett 12:281